DOI: 10.1002/ejic.200501089

Proton-Coupled Redox Chemistry, Oxidative Reactivity, and Electronic Characterization of Aqua-, Hydroxo-, and Oxo-Triruthenium Clusters

Genebaldo S. Nunes,[a] Anamaria D. P. Alexiou,[a] Koiti Araki,[a] André L. B. Formiga,[a] Reginaldo C. Rocha,*[b] and Henrique E. Toma*[a]

Keywords: Ruthenium–acetate clusters / Mixed-valence complexes / Oxygen-transfer catalysis / Proton-coupled electron transfer / Pourbaix diagram / Electrocatalysis / Spectroelectrochemistry

The pH-dependent electronic and electrochemical properties of a series of triangular μ_3-oxo-centered trinuclear clusters of the type $[Ru_3O(Ac)_6(py)_2(OH_x)]^n$ (Ac = acetate; py = pyridine; x = 0, 1, or 2; where the formal oxidation states on the metal ions range from +II to +IV) have been investigated with emphasis on the elucidation of the successive proton-coupled redox processes spanning the interconvertible aqua- (x = 2), hydroxo- (x = 1), and oxo- (x = 0) forms, from which the complete Pourbaix diagram has been proposed. From the spontaneous slow coupling reaction of the monomeric cluster in its deprotonated (oxo) form at high pH, the μ-oxo-bridged cluster dimer (i.e. $\{(py)_2(Ac)_6ORu_3\}$-O-$\{Ru_3O(Ac)_6(py)_2\}$) has been isolated and fully characterized by spectroelectrochemistry as well. A further understanding of the underlying electronic interactions across the various oxidation and protonation states, and the role of such phenomena in the activation of the Ru–O bonding system in oxygen-transfer catalysis, have also been explored.

Introduction

The chemistry of water as a ligand in coordination compounds can be rather puzzling when the metal ions display many successive oxidation states.[1] That is mostly because, in such systems, the ligand acid–base behavior and metal-centered redox properties are coupled and, therefore, proton and electron transfer can simultaneously occur in connection with chemical and electronic transformations in the complex. The consequences of this type of dynamic synergism called proton-coupled electron transfer (PCET) are, in many different aspects, widespread in synthetic and natural systems (e.g. from sol-gel processes in materials chemistry to photosynthetic oxygen evolution in green plants).[2,3]

In the particular context of model systems towards (electro)catalytic oxidation of organics, a remarkable series of (polypyridyl)ruthenium complexes involving oxidation-state/pH-dependent equilibrium PCET reactions of the type H_2O–$Ru^{II} \rightleftharpoons$ HO–$Ru^{III} \rightleftharpoons$ O=Ru^{IV} (i.e. aqua, hydroxo, and oxo forms, respectively), has been largely investigated by Meyer and co-workers.[4] In the light of those studies, an extraordinary chemistry has been revealed from the apparently simple Ru–O structure. In addition to the complexity introduced by the multiple ligand-based protonation states coexisting with the metal-based oxidation states, a detailed understanding of the underlying metal–ligand interactions can be especially challenging when metal–metal electronic coupling is also involved, as in the case of the triangular μ-oxo-centered triruthenium clusters $[Ru_3O(Ac)_6(py)_2(OH_x)]^n$ (Ac = acetate ion, py = pyridine), focused herein (Scheme 1, a).

The trinuclear ruthenium complexes of the type $[Ru_3O(Ac)_6(L)_3]^n$ and $[Ru_3O(Ac)_6(L)_2(L')]^n$ (where L is usually a pyridyl ligand) have been extensively investigated[5] since the seminal work by Wilkinson[6,7] and Meyer[8,9] and co-workers, on the mixed-valence properties of the Ru_3O cluster core. In addition to the metal–metal bonding, the triangular center is strongly held by six acetate bridges and a central oxygen atom (oxo) that is capable of interacting with up to three empty Ru d_π orbitals. When L′ is H_2O, its acid–base properties are expected to be sensitive to the redox states of the Ru ions and, to some extent, the electronic coupling within the trinuclear cluster core. There is also the possibility of forming oxo-bridged dimers (Scheme 1, b), expanding the influence of the mixed-valence interactions over the entire polymetallic system. All these aspects have been investigated in this work, with especial emphasis on the elucidation of the proton-coupled redox processes by electrochemical and spectroelectrochemical methods. Further, the role of intermetallic electronic interactions in the activation of the Ru–O bonding structure in oxygen-transfer catalysis has also been explored.

[a] Instituto de Química, Universidade de São Paulo, C.P. 26077, CEP 05513-970, São Paulo, SP, Brazil
E-mail: henetoma@iq.usp.br
[b] Los Alamos National Laboratory, Mail Stop G755, Los Alamos, NM 87545, USA
E-mail: rcrocha@lanl.gov

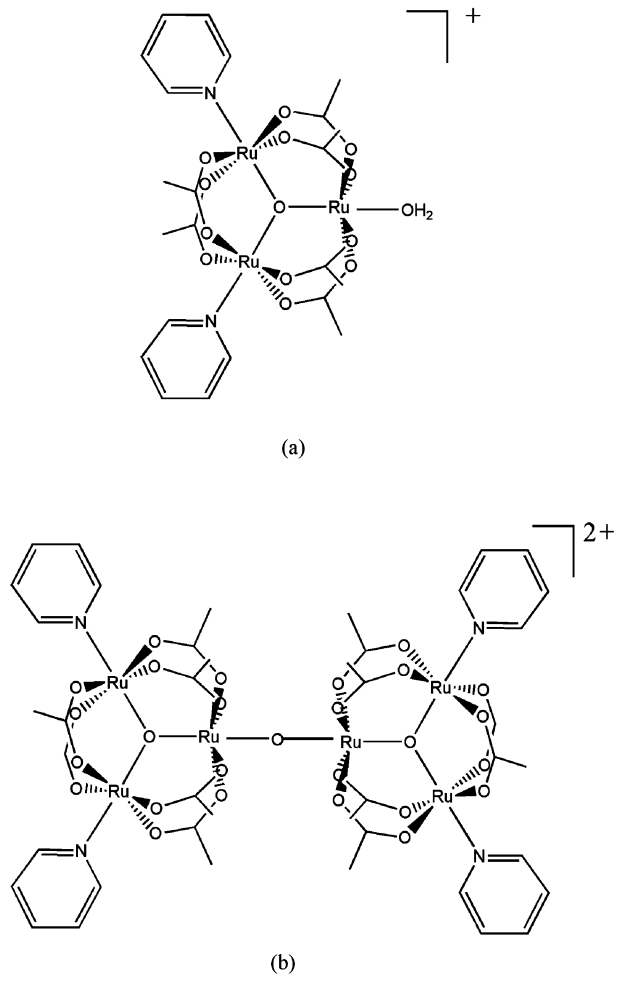

Scheme 1. Structural formulas of (a) the cluster $[Ru_3O(Ac)_6(py)_2(H_2O)]^+$ and (b) the oxo-bridged cluster dimer $[\{Ru_3O(Ac)_6(py)_2\}_2(\mu\text{-}O)]^{2+}$.

Results and Discussion

Electronic Absorption Spectra

The electronic spectra of the $[Ru_3^{III,III,III}O(Ac)_6(py)_2(H_2O)]^+$ complex in aqueous solution, at various pH values, are shown in Figure 1. In general, a characteristic set of absorption bands is observed at 498 (ε = 1630), 607 (ε = 3390), and 683 nm (ε = 4300), in addition to a shoulder near 390 nm. The main visible absorption envelope and the higher-energy shoulder have been associated to intracluster (IC) metal–metal electronic transitions and $Ru_3O(d_\pi)\rightarrow py(\pi^*)$ charge-transfer (CT) transitions, respectively, on the basis of previous detailed assignments.[5,9–11]

As shown in Figure 1, no spectral change is observed in the pH range of 1.9–6.5. Above pH 6.5, a systematic spectral shift of the IC bands to 592, 702, and ≈808 nm occurs, accompanied by two isosbestic points at 577 and 712 nm. In the pH range of 6.5–11.5, the process is essentially reversible, corresponding to the acid–base equilibrium of Equation (1).

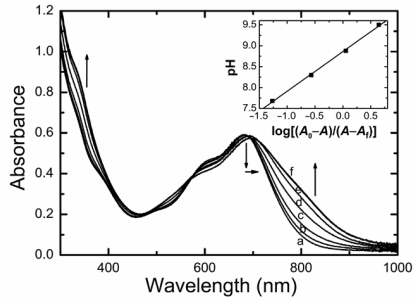

Figure 1. Eletronic spectra of $[Ru_3O(Ac)_6(py)_2(H_2O)]^+$ ($1.4\cdot10^{-4}$ M) in BR buffer at various pH values: (a) 1.9–6.5; (b) 7.7; (c) 8.3; (d) 8.9; (e) 9.5; and (f) 11.1 and 12.0. Inset: pH vs. $\log[(A_0 - A)/(A - A_f)]$, where A is the measured absorbance at any given pH, A_0 is the starting absorbance at the lowest pH, and A_f is the final absorbance at the highest pH.

$$[Ru_3^{III,III,III}O(Ac)_6(py)_2(H_2O)]^+ \rightleftharpoons [Ru_3^{III,III,III}O(Ac)_6(py)_2(OH)] + H^+ \quad (1)$$

From the linear plot of pH vs. $\log[(A_0 - A)/(A - A_f)]$ (Figure 1; inset), the pK_a for the process given in Equation (1) was calculated to be 8.86 (±0.02). It is interesting to notice that the K_a of the aqua ligand in the $[Ru_3^{III,III,III}O(Ac)_6(py)_2(H_2O)]^+$ species herein is about four orders of magnitude smaller than that previously reported for the $[Ru_3^{III,III,III}O(Ac)_6(OH)_2(H_2O)]^-$ species (pK_a > 12).[5,6] This observation reflects the influence of the π-backbonding ability of the pyridine ligands, in contrast with the hydroxo ligands. Also, considering that the pK_a of the $[Ru(bpy)_2(py)(H_2O)]^{3+}$ complex is 0.85,[12] the dominant role of the metal–metal interactions in the trinuclear Ru^{III} cluster becomes quite evident. Actually, the presence of the strong bonding and delocalization within the Ru_3O core provides an electronic environment that closely resembles that of mononuclear Ru^{II} complexes such as $[Ru(bpy)_2(py)(H_2O)]^{2+}$ and *trans*-$[Ru(bpydip)(H_2O)_2]^{2+}$ [where bpy is 2,2′-bipyridine, and bpydip is a tetradentate Schiff base ligand, *N*,*N*′-bis(7-methyl-2-pyridylmethylene)-1,3-diiminopropane], as deduced from their pK_a of 10.6 and 8.9, respectively.[4,13]

By monitoring the electronic spectra of the hydroxo, neutral $[Ru_3^{III,III,III}O(Ac)_6(py)_2(OH)]$ species as a function of time (Figure 2), it was observed that the systematic decrease of the absorption band around 700 nm occurs simultaneously with the rise of a broad band around 900 nm, which is characteristic of the aqua cluster $[Ru_3^{III,III,II}O(Ac)_6(py)_2(H_2O)]$ (as demonstrated below by spectroelectrochemistry). Therefore, as shown in Equation (2), the hydroxo-[III,III,III] species slowly disproportionates, at high pH, generating the corresponding protonated/reduced (aqua-[III,III,II]) and deprotonated/oxidized (oxo-[IV,III,III]) forms.

Figure 2 (b) shows the corresponding kinetics for the disproportionation reaction of Equation (2). The initial rates measured at 700 nm $(1.04\pm0.02)\cdot10^{-5}$ s^{-1} and 900 nm $(1.98\pm0.03)\cdot10^{-5}$ s^{-1}, were in excellent agreement with the theoretical relationship of Equation (3).

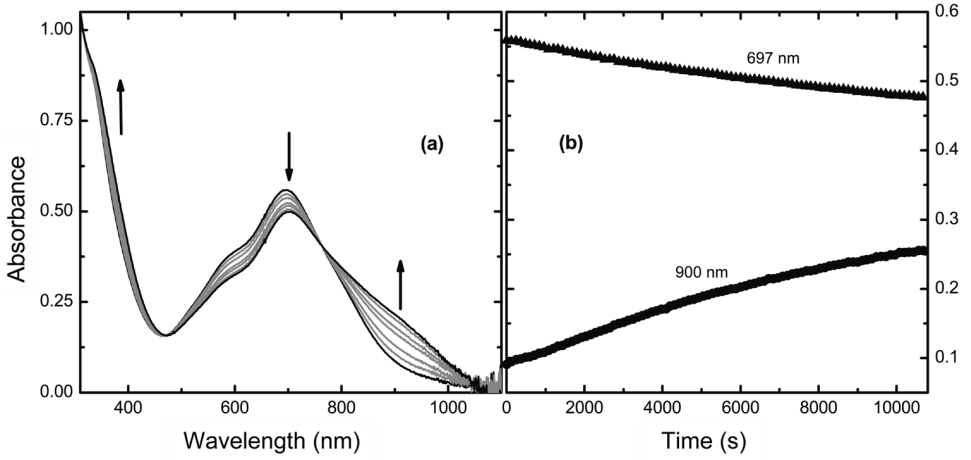

Figure 2. (a) Spectral changes of $[Ru_3O(Ac)_6(py)_2(H_2O)]^+$ ($1.4 \cdot 10^{-4}$ M) in BR buffer at pH 11.4, as a function of time; (b) absorbance changes at 697 and 900 nm as a function of time.

$$2\ [Ru_3^{III,III,III}O(Ac)_6(py)_2(OH)] \rightleftharpoons [Ru_3^{III,III,II}O(Ac)_6(py)_2(OH_2)] + [Ru_3^{IV,III,III}O(Ac)_6(py)_2(O)] \quad (2)$$

$$-(1/2)\ d[Ru_3^{III,III,III}(OH)]/dt = d[Ru_3^{III,III,II}(OH_2)]/dt \quad (3)$$

In order to evaluate the end point of the reaction, the sample undergoing disproportionation was kept in the dark for 24 h and, then, the spectra were measured again at several pH values (Figure 3). The major differences (relative to the spectra of Figure 2, a) were observed above pH 11; i.e., the main absorption band was shifted from 683 nm to 702 nm, and there was an enhancement of the absorption at 343 nm. In addition, the lack of isosbestic points indicates the occurrence of further reactions following the disproportionation process.

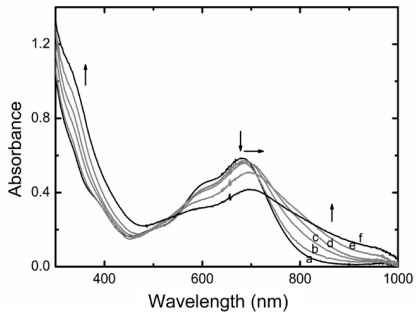

Figure 3. Eletronic spectra of $[Ru_3O(Ac)_6(py)_2(H_2O)]^+$ ($1.4 \cdot 10^{-4}$ M) in BR buffer at various pH values: (a) 1.9; (b) 8.3; (c) 8.9; (d) 9.5; (e) 11.1; (f) 12.0. The sample solution was prepared 24 h prior to the measurements.

By treating the solution (aged for 24 h at pH 12) with diethyl ether, only the neutral aqua cluster, i.e. $[Ru_3^{III,III,II}O(Ac)_6(py)_2(OH_2)]$, could be detected in the organic fraction, as shown in Figure 4, a (see below for detailed assignments).

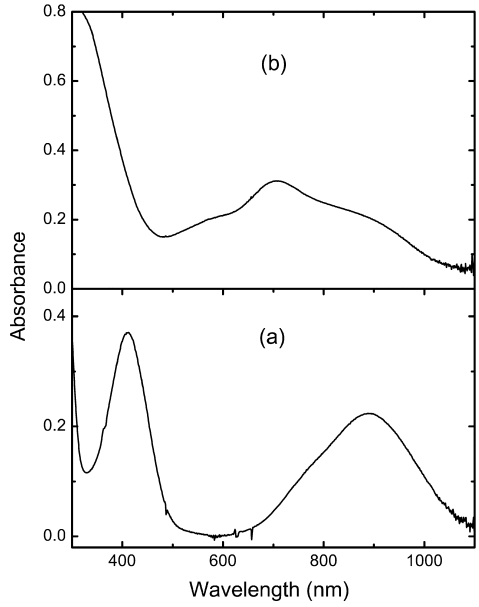

Figure 4. Electronic spectra of (a) the diethyl ether fraction containing the reduced aqua species, $[Ru_3^{III,III,II}O(Ac)_6(py)_2(OH_2)]$, and (b) the remaining, previously ether-treated aqueous solution at pH 12.0 (BR buffer, 0.1 M).

The spectrum of the ether-treated aqueous solution (Figure 4, b) exhibits absorption bands at 893, 712, 566 and 343 nm. In principle, according to the disproportionation reaction of Equation (2), before the extraction with ether the reaction mixture should also contain the oxo species, $[Ru_3^{IV,III,III}O(Ac)_6(py)_2(O)]$, and perhaps some remainder of the starting hydroxo species, $[Ru_3^{III,III,III}O(Ac)_6(py)_2(OH)]$. However, although these are both electrically neutral species, none of these forms could be detected in the extracted organic phase containing the aqua counterpart. A plausible explanation for this observation is that, after aging for 24 h at pH > 11, the $[Ru_3^{IV,III,III}O(Ac)_6(py)_2(O)]$ species would dimerize into $[\{Ru_3^{IV,III,III}O(Ac)_6(py)_2\}_2(O)]^{2+}$

[Equation (4)], analogously to the previously reported for the $[Ru(bpy)_2(py)(O)]^{2+}$ complex.[14]

$$2\ [Ru_3^{IV,III,III}O(Ac)_6(py)_2(O)] + H_2O \rightleftharpoons [\{Ru_3^{IV,III,III}O(Ac)_6(py)_2\}_2(O)]^{2+} + 2\ OH^- \quad (4)$$

Alternatively, the oxo-[IV,III,III] species could react with any remaining amount of the cluster in the hydroxo-[III,III,III] form to yield the mixed-valent dimer, as shown in Equation (5).

$$[Ru_3^{IV,III,III}O(Ac)_6(py)_2(O)] + [Ru_3^{III,III,III}O(Ac)_6(py)_2(OH)] \rightleftharpoons [(py)_2(Ac)_6ORu_3^{IV,III,III}(O)Ru_3^{III,III,III}O(Ac)_6(py)_2]^+ + OH^- \quad (5)$$

In order to obtain additional evidence on the formation of such dimeric species, the final product was further isolated and characterized as follows. The starting $[Ru_3^{III,III,III}O(Ac)_6(py)_2(H_2O)]Cl$ compound was dissolved in a minimum volume of water and treated with an equimolar amount of NaOH. After 24 h, the one-electron reduced, neutral species (H_2O-[III,III,II]) was extracted from the mixture with diethyl ether (as above), and the treated aqueous solution was evaporated to dryness. Mass spectra (ESI-MS; see Exp. Sect. for details) of the product, in methanol, exhibited a main peak at $m/z = 1751$, consistent with the $[\{Ru_3O(Ac)_6(py)_2\}_2(O)]Cl_2^+$ formulation ($m/z = 1751$) which, therefore, corresponds to the μ-oxo-bridged mixed-valent [IV,IV,III–IV,III,III] cluster dimer after ionization in gas phase. It is worth noting that the chloride ions were present as counterions because the cluster dimer was generated from the starting $[Ru_3O(Ac)_6(py)_2(H_2O)]Cl$ complex. Isolation of the dimeric species in pure form (using conventional liquid chromatography) has not yet been accomplished because such species seems to undergo facile interconversion between the mixed-valence states, as confirmed by the ESI-MS experiments.

Electrochemical Behavior

Typical cyclic voltammograms of the $[Ru_3O(Ac)_6(py)_2(H_2O)]^+$ cluster in aqueous solution, at three representative pH values, are shown in Figure 5. A characteristic reversible wave, assigned to the Ru-centered III,III,III/III,III,II redox couple, was observed with $E_{1/2} = 0.20$ V (vs. SHE); Equation (6). Above pH 8, the process exhibits a pH-dependent, Nernstian behavior with E^o (V vs. SHE) = 0.20 – 0.059·pH. The pK_a associated with the equilibrium of Equation (7) was evaluated from the Pourbaix ($E_{1/2}$ vs. pH) plot shown in Figure 6, with the determined value of 8.7 in agreement with that obtained by spectrophotometry (8.86) as above.

$$[Ru_3^{III,III,III}(H_2O)]^+ + e \rightleftharpoons [Ru_3^{III,III,II}(H_2O)] \quad E_{1/2} = 0.20\ V \quad (6)$$

$$[Ru_3^{III,III,III}(H_2O)]^+ \rightleftharpoons [Ru_3^{III,III,III}(OH)] + H^+ \quad pK_a = 8.8 \quad (7)$$

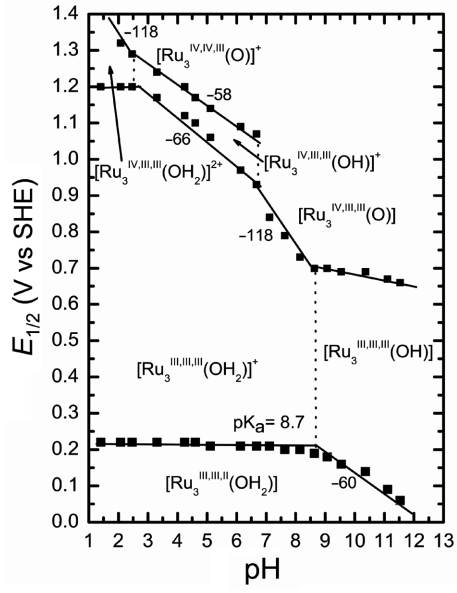

Figure 6. Pourbaix diagrams for $[Ru_3O(Ac)_6(py)_2(OH_x)]^n$ in aqueous solution; pK_a values and slopes (given in mV) are also noted in the Figure. At pH > 9 and $E^o > 1.0$ V, the dimeric species (not shown) predominate; see text for details.

The corresponding spectral changes accompanying the above redox transformations are shown in Figure 7. The electrochemical III,III,III/III,III,II reduction of the aqua cluster at pH 6.7 proceeds reversibly, generating the characteristic cluster-core IC bands with λ_{max} around 890 nm and the $Ru_3O(d_\pi) \rightarrow py(p_\pi^*)$ CT band at 364 nm.

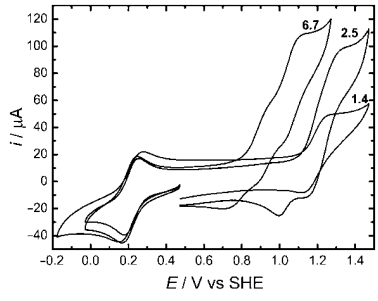

Figure 5. Cyclic voltammograms (at 50 mV s^{-1}) of $[Ru_3O(Ac)_6(py)_2(H_2O)]^+$ ($1.3 \cdot 10^{-3}$ M) in BR buffer/NaTFA (0.1 M) at pH 1.4, 2.5, and 6.7.

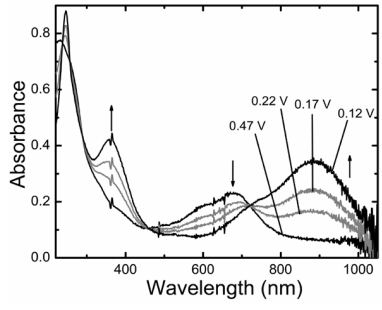

Figure 7. Spectroelectrochemical changes in a solution of $[Ru_3O(Ac)_6(py)_2(H_2O)]^n$ ($1.9 \cdot 10^{-3}$ M), at pH 6.7 [BR buffer/NaTFA (0.1 M)], in the potential range of 0.47 V ($Ru_3^{III,III,III}$; $n = 1+$) to 0.12 V ($Ru_3^{III,III,II}$; $n = 0$).

At pH 1.4, the cyclic voltammograms display another reversible wave at 1.2 V (Figure 5), corresponding to the IV,III,III/III,III,III redox couple [Equation (8)], which is dramatically sensitive to pH changes. The Pourbaix plots (Figure 6) exhibit two breaking points at pH 2.5 and 6.7, which correspond to the pK_a's of the equilibria in Equation (9) and Equation (10), respectively.

$$[Ru_3^{IV,III,III}(H_2O)]^{2+} + e \rightleftharpoons [Ru_3^{III,III,III}(H_2O)]^{+} \quad E_{1/2} = 1.20\ V \quad (8)$$

$$[Ru_3^{IV,III,III}(H_2O)]^{2+} \rightleftharpoons [Ru_3^{IV,III,III}(OH)]^{+} + H^{+} \quad pK_a = 2.5 \quad (9)$$

$$[Ru_3^{IV,III,III}(OH)]^{+} \rightleftharpoons [Ru_3^{IV,III,III}(O)] + H^{+} \quad pK_a = 6.7 \quad (10)$$

Because the required potentials for the oxidation of the $[Ru_3^{III,III,III}O(Ac)_6(py)_2(H_2O)]^+$ species were near the working limits of water, the formation of the IV,III,III redox state could not be monitored spectroelectrochemically. Instead, a spectrophotometric redox titration was carried out in $HClO_4$ (0.1 M) using Ce^{IV} as a chemical oxidant. As shown in Figure 8 (b), the redox titration was consistent with a 1:1 stoichiometry. The oxidized $[Ru_3^{IV,III,III}O(Ac)_6(py)_2(H_2O)]^{2+}$ species exhibits two characteristic IC bands at 565 and 776 nm, as shown in Figure 8 (a).

At pH 2.5, an additional oxidation wave was discernible at 1.3 V, overlapping the existing reversible wave with $E_{1/2}$ = 1.2 V. The intensity of the resulting convoluted wave was two times that of a monoelectronic process. The new cathodic wave is pH-dependent and was assigned to the 1-H^+ or 2-H^+ proton-coupled IV,IV,III/IV,III,III redox process of Equation (11) or Equation (12), respectively, depending on the pH region (Figure 6).

$$[Ru_3^{IV,IV,III}(O)]^{+} + 2\,H^{+} + e^{-} \rightleftharpoons [Ru_3^{IV,III,III}(OH_2)]^{2+} \quad pH < 2.5 \quad (11)$$

$$[Ru_3^{IV,IV,III}(O)]^{+} + H^{+} + e^{-} \rightleftharpoons [Ru_3^{IV,III,III}(OH)]^{+} \quad pH > 2.5 \quad (12)$$

The overall redox processes discussed above have been collected in the Pourbaix diagrams of Figure 6.

It should be noted that at pH 6.7 the spectroelectrochemical oxidation (Figure 9) of $[Ru_3^{III,III,III}O(Ac)_6(py)_2(H_2O)]^+$, starting from 0.47 V, actually involves two overlapping successive redox processes. At 0.97 V, the hydroxo species $[Ru_3^{IV,III,III}O(Ac)_6(py)_2(OH)]^+$ should be predominantly formed; at 1.12 V, the product of oxidation (coupled to deprotonation) is expected to be $[Ru_3^{IV,IV,III}O(Ac)_6(py)_2(O)]^+$. A new band at 418 nm was observed for the latter, in addition to a broad band around 850 nm. On the other hand, the vestiges of the initial band around 700 nm may be an indication of some partial regeneration of the starting complex, perhaps by a parallel catalytic process involving the decomposition of water by the highly oxidized, oxo-[IV,IV,III] species (a point that will be discussed below).

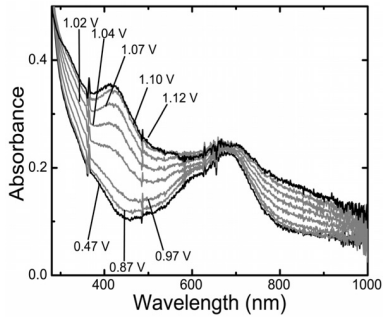

Figure 9. Spectroelectrochemical changes in a solution of $[Ru_3O(Ac)_6(py)_2(OH_x)]^+$ ($1.9\cdot10^{-3}$ M), at pH 6.7 [BR buffer/NaTFA (0.1 M)], in the potential range of 0.47 V (aqua-$Ru_3^{III,III,III}$) to 0.97 V (hydroxo-$Ru_3^{IV,III,III}$), and then to 1.12 V (oxo-$Ru_3^{IV,IV,III}$).

At pH 9.5 a different electrochemical pattern is observed (Figure 10), with three oxidation waves in the 0.7–1.2 V range. The anodic process at 0.73 V seems to follow a regular pattern when it is inserted into the Pourbaix diagram (Figure 6), and is consistent with the proton-coupled redox process of Equation (13).

$$[Ru_3^{III,III,III}(OH)] + OH^{-} \rightarrow [Ru_3^{IV,III,III}(O)] + H_2O + e^{-} \quad (13)$$

The remaining anodic peaks around 1.0 V exhibit relative intensities strongly dependent on the potential scan rates, indicating the occurrence of chemical reactions coupled with the oxidation of the $[Ru_3^{IV,III,III}O(Ac)_6(py)_2(O)]$ species (into $[Ru_3^{IV,IV,III}O(Ac)_6(py)_2(O)]^+$). A possibility is the decomposition of water by the oxo-[IV,IV,III] species [Equation (14)], which accounts for the catalytic peak mani-

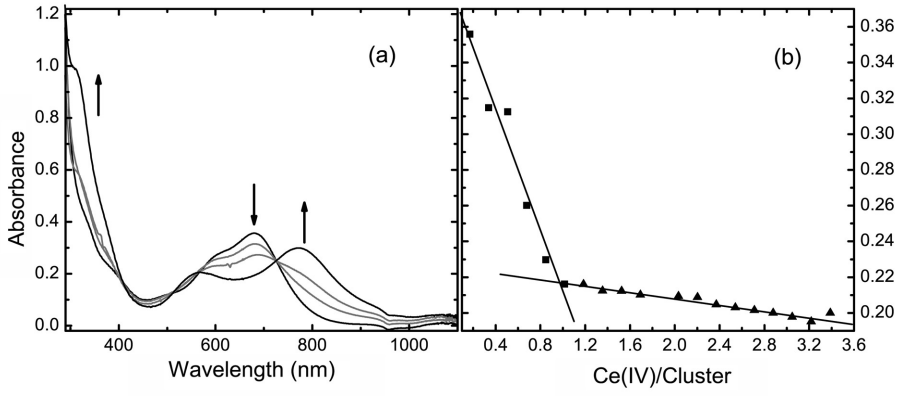

Figure 8. (a) Spectrophotometric redox titration of $[Ru_3O(Ac)_6(py)_2(H_2O)]^+$ ($1.0\cdot10^{-4}$ M) in $HClO_4$ (0.1 M) with Ce(IV) in H_2SO_4 (1.0 M). (b) Plot of absorbance (at 683 nm) vs. Ce(IV)/cluster molar ratio.

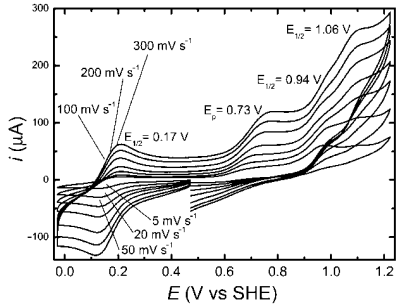

Figure 10. Cyclic voltammograms, at several scan rates, of $[Ru_3O(Ac)_6(py)_2(H_2O)]^+$ ($1.3\cdot10^{-3}$ M) in BR buffer/NaTFA (0.1 M) at pH 9.5.

fested near 1.0 V at low scan rates (Figure 10). This reaction regenerates the starting aqua-[III,III,III] species, thus explaining the lack of cathodic waves in the reverse scan.

$$2\ [Ru_3^{IV,IV,III}(O)]^+ + 2\ H_2O \rightarrow 2\ [Ru_3^{III,III,III}(H_2O)]^+ + O_2 \qquad (14)$$

By increasing the scan rates, two inflections can be noted around 0.95 and 1.15 V, in addition to the catalytic wave. As shown below, these signals can be assigned to the presence of small amounts of dimeric species. In fact, cyclic voltammograms of the product isolated from the disproportionation reaction discussed above, in acetonitrile (Figure 11), are consistent with the existence of dimeric species.

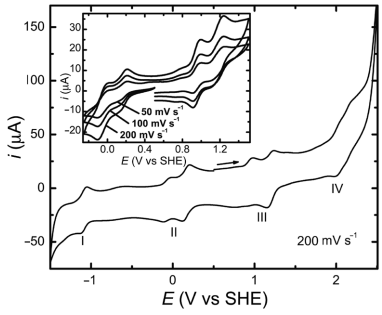

Figure 11. Cyclic voltammograms of the cluster dimer $[\{Ru_3O(Ac)_6(py)_2\}_2(O)]^{2+}$ ($1.9\cdot10^{-3}$ M) in acetonitrile/TEAP (0.1 M).

The voltammograms of the cluster dimer in acetonitrile exhibit essentially the characteristic waves for the cluster monomer "in duplicate". Table 1 summarizes the corresponding processes in four distinct regions: (I) –1.09 V; (II) –0.07 and 0.16 V; (III) 0.95 and 1.17 V; (IV) 2.01 and 2.14 V (see also Figure 11).

Table 1. Redox potentials for the oxo-bridged cluster dimer, $[\{Ru_3O(Ac)_6(py)_2\}_2(O)]^n$, in acetonitrile/TEAP (0.1 M).

Redox couple (Ru_3–Ru_3)	$E_{1/2}$ (V vs. SHE)
[III,III,II]–[III,III,II]/2[III,II,II]	–1.09
[III,III,III]–[III,III,II]/[III,III,II]–[III,III,II]	–0.07
[III,III,III]–[III,III,III]/[III,III,III]–[III,III,II]	0.16
[IV,III,III]–[III,III,III]/[III,III,III]–[III,III,III]	0.95
[IV,III,III]–[IV,III,III]/[IV,III,III]–[III,III,III]	1.17
[IV,IV,III]–[IV,III,III]/[IV,III,III]–[IV,III,III]	2.01
[IV,IV,III]–[IV,IV,III]/[IV,IV,III]–[IV,III,III]	2.14

The reversible waves observed at 0.95 and 1.17 V are consistent with those obtained in aqueous solution at pH 9. From the splitting of the redox couples involving mixed-valent states, the comproportionation constant for the $[Ru_3–Ru_3]^n + [Ru_3–Ru_3]^{n+2} \rightleftharpoons 2\times[Ru_3–Ru_3]^{n+1}$ equilibrium can be calculated as $K_c = \exp[(\Delta E\cdot F)/RT]$,[15] where ΔE is the potential separation between the $[Ru_3–Ru_3]^{n+2}/[Ru_3–Ru_3]^{n+1}$ and $[Ru_3–Ru_3]^{n+1}/[Ru_3–Ru_3]^n$ redox couples (i.e., $\Delta E_{1/2}$). In this way, the obtained values for regions II–IV are: $7.7\cdot10^3$ (ΔE = 230 mV; region II), $5.2\cdot10^3$ (ΔE = 220 mV; region III) and $1.6\cdot10^2$ (ΔE = 130 mV; region IV). As comproportionation constants can be related to the stabilization promoted by the electronic delocalization in the mixed-valence states,[15] according to this evaluation of K_c based on the closely-spaced redox potentials, the electronic coupling between the two cluster units does not appear to be particularly strong within the oxidation-state range studied and reported herein. Consistent with these findings are also preliminary results of ongoing theoretical calculations of molecular and electronic structures, which provide additional evidence for the moderate extent of cluster-to-cluster electronic communication (despite the obvious metal–ligand mixing and delocalization within each cluster).

Attempts to detect the existence of cluster-to-cluster intervalence charge-transfer (IVCT) bands in the mixed-valence states of the cluster dimer were conducted by means of Vis/near-IR spectroelectrochemistry in acetonitrile, in the potential range of –1.0 to 1.2 V. Unfortunately, the results were not conclusive, resembling those of the monomeric species. No evidence of such IVCT transitions was found, most likely due to weak absorptivity or convolution with the broad IC bands.

Electrocatalytic Activity in the Oxidation of Benzyl Alcohol

Oxo–metal complexes are of great interest in the catalytic oxidation of organic substrates[16–31] because of their ability to promote selective oxygen-transfer reactions, without the participation of less specific oxygen-free radical agents.[24,29,30] For this reason, we extended the study on the redox properties of the oxo–ruthenium clusters to include their electrocatalytic behavior in the oxidation of benzyl alcohol in aqueous solution.

Figure 12 shows typical cyclic voltammograms of the $[Ru_3^{III,III,III}O(Ac)_6(py)_2(H_2O)]^+$ complex in aqueous solution, at pH 3.0, in the presence of increasing amounts of benzyl alcohol. A linear increase of the amperometric current is observed at 1.2 V, which coincides with the convoluted waves assigned above to the proton-coupled oxidation of $[Ru_3^{III,III,III}O(Ac)_6(py)_2(H_2O)]^+$ into $[Ru_3^{IV,III,III}{}_3O(Ac)_6(py)_2(OH)]^+$ and $[Ru_3^{IV,IV,III}O(Ac)_6(py)_2(O)]^+$. The lack of redox response from the benzyl alcohol up to 1.4 V, and the absence of the cathodic waves from the oxidized clusters in the reverse scan, are consistent with the electrocatalytic oxidation of benzyl alcohol.

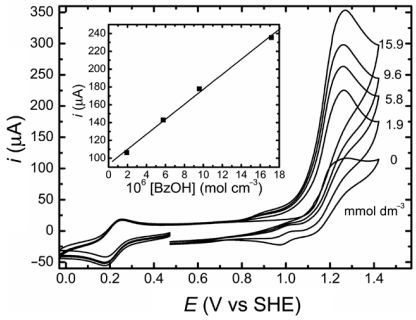

Figure 12. Cyclic voltammograms (at 50 mV s^{-1}) of $[Ru_3O(Ac)_6(py)_2(H_2O)]^+$ ($1.3\cdot10^{-3}$ M) in BR buffer/NaTFA (0.1 M), at pH 3.0, in the presence of various amounts of benzyl alcohol. The inset shows the linear dependence of the anodic peak current above 1.2 V vs. the concentration of benzyl alcohol.

Additional insight into the electrocatalytic oxidation of benzyl alcohol was obtained from the cyclic voltammograms of similar sample solutions at pH 6.7 (Figure 13). In this case, the pH-dependent reduction potential of the hydroxo-[IV,III,III]/aqua-[III,III,III] redox/protonation couple was shifted to 0.9 V. From the current increase at 1.1 V,

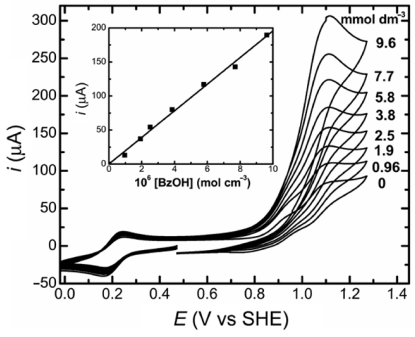

Figure 13. Cyclic voltammograms (at 50 mV s^{-1}) of $[Ru_3O(Ac)_6(py)_2(H_2O)]^+$ ($1.3\cdot10^{-3}$ M) in BR buffer/NaTFA (0.1 M), at pH 6.7, in the presence of various amounts of benzyl alcohol. The inset shows the linear dependence of the anodic peak current around 1.1 V vs. the concentration of benzyl alcohol.

the catalytic wave can be readily associated with participation of the oxo-[IV,IV,III]/hydroxo-[IV,III,III] couple.

The electrocatalytic scheme in this case corresponds to that categorized by Nicholson and Shain[32] as type VII, which involves a reversible electron transfer followed by a reaction regenerating the starting complex [Equation(15)].

$$R \rightleftharpoons O + ne^- \quad (15a)$$

$$O + Z \rightarrow R\ (k'_f) \quad (15b)$$

For this scheme, assuming a diffusional process for the catalytic reaction, Sawyer[33] has shown that, when the scan rates increase by an order of magnitude, the peak potential (E_p) is shifted by approximately 0.030 V, as expressed by Equation (16) (where α is the electron-transfer coefficient, n_α is the number of electrons involved in the process, and v is the potential scan rate). From the slope of the linear plot in Figure 14 (a), $\alpha\cdot n_\alpha = 0.91$. Similarly, by combining this value into Equation (17)[32,33] (where i_p is the oxidation peak current, A is the electrode area, C_0 is the substrate concentration, and the diffusion coefficient, $D_0 = 7.1\cdot10^{-6}$ $cm^2 s^{-1}$, was estimated from the Stokes-Einstein[25] equation: $D = k_B T/6\pi r\eta$, k_B = Boltzmann's constant, T = temperature, r = solvodynamic radius, and η = viscosity), the number of electrons n was calculated to be 2.04 from the slope of the corresponding linear plot shown in Figure 14 (b). Therefore, the oxidation of benzyl alcohol proceeds by a two-electron-transfer process to generate benzaldehyde, as also confirmed by standard tests with (2,4-dinitrophenyl)hydrazine.

$$E_p = K + (0.03/\alpha\cdot n_\alpha)\log(v) \quad (16)$$

$$i_p = 2.99\cdot10^5\, n\, (\alpha\cdot n_\alpha)^{1/2}\, A\cdot C_0\cdot D_0^{1/2}\cdot v^{1/2} \quad (17)$$

The catalytic kinetic constant (k_f) can be determined from the working plot of i_k/i_d vs. $\psi^{1/2}$ (where i_k is the catalytic current, i_d is the diffusion current, $\psi = k_f/a$ and $a = nFv/RT$), as described by Nicholson and Shain[32] (Figure 15, a). The catalytic current, in this case, was measured in the presence of benzyl alcohol under pseudo-first-order conditions ($C = 9.6\cdot10^{-3}$ M). The diffusion current was given

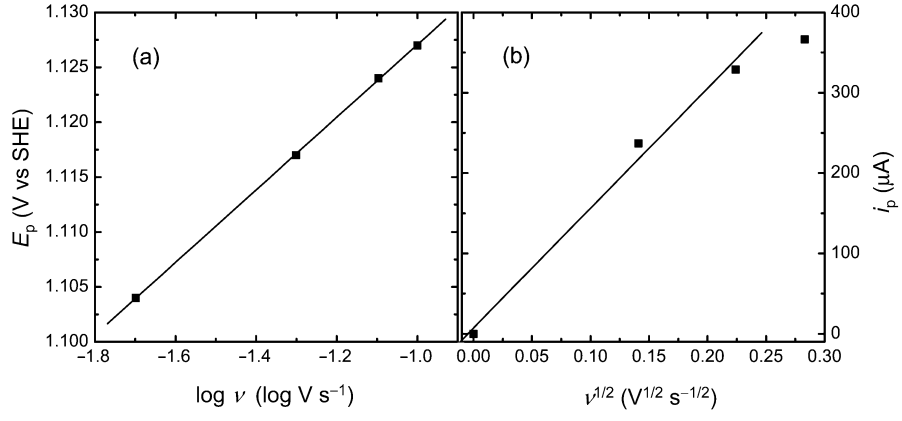

Figure 14. Plots of the catalytic potential peak vs. log$v$ (a) or catalytic current peak vs. $v^{1/2}$ (b), for the oxidation of benzyl alcohol ($3.85\cdot10^{-3}$ M) by the cluster ($1.3\cdot10^{-3}$ M) at pH 6.7 [BR buffer/NaTFA (0.1 M)].

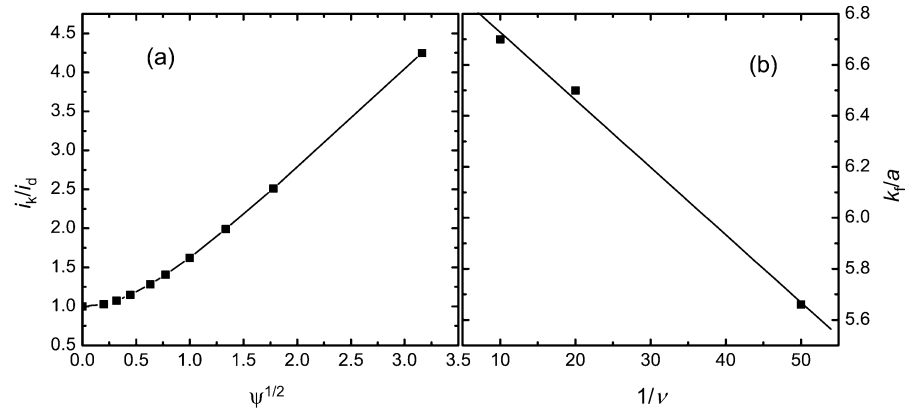

Figure 15. Plots of (a) i_k/i_d vs. $\psi^{1/2}$, and (b) k_f/a vs. $1/\nu$ (see text for details).

by the same measurement in the absence of the substrate. The calculated $k_f/_a$ values are then plotted against $1/\nu$ and, from the slope, $k_f/(nF/RT)$ is obtained. In this way, k_f was determined to be 2.1 s^{-1} and, the corresponding second-order rate constant, $k'_f = k_f/[\text{substrate}]$, is $2.2 \cdot 10^2$ M^{-1} s^{-1}.

It is interesting to notice that the kinetic constant for the oxidation of benzyl alcohol by the cluster is significantly higher than those reported[34] for the complexes $[Ru^{IV}(tpy)(bpy)(O)]^{2+}$, at pH 13, ($k'_f$ = 36.1 M^{-1} s^{-1}) or $[Ru^{IV}(tpy)(bpz)(O)]^{2+}$ (k'_f = 23.0 M^{-1} s^{-1}), at pH 11 (tpy = 2,2′′:6,2′′-terpyridine; bpz = 2,2′-bipyrazine). Considering the redox potentials for these complexes (0.86 V and 0.90 V, respectively),[34,35] the comparatively enhanced catalytic activity of the $[Ru_3^{IV,IV,III}O(Ac)_6(py)_2(O)]^+$ cluster may arise from its stronger oxidizing character (E^o = 1.1 V at pH 6.7).

Conclusion

In summary, the trinuclear ruthenium clusters of the type $[Ru_3O(Ac)_6(py)_2(OH_x)]^n$ exhibit a very rich proton-coupled redox chemistry in aqueous solution. On the basis of cyclic voltammetry and spectroelectrochemical measurements as a function of pH, the various protonation/oxidation states have been characterized and the complete Pourbaix diagram has been proposed for the system, which comprises all reversible one-proton/one-electron transformations involving the aqua- (x = 2), hydroxo- (x = 1), and oxo- (x = 0) forms with the increasing oxidation states of the triangular redox center. An enhanced catalytic activity for the $[Ru_3^{IV,IV,III}O(Ac)_6(py)_2(O)]^+$ oxo species has been demonstrated in the oxidation of benzyl alcohol, evidencing the activation of the Ru^{IV}–O bonding in oxygen-transfer reactions. Moreover, the new μ-oxo-bridged cluster dimer $[\{(py)_2(Ac)_6ORu_3\}\text{-}O\text{-}\{Ru_3O(Ac)_6(py)_2\}]^n$ has been isolated and characterized, and the combined electrochemical and spectroscopic results indicate only moderate electronic coupling between the two triangular cluster units through the oxo bridge. Next, additional understanding of the molecular and electronic structures of these systems will also be pursued by means of theoretical quantum chemical calculations, which should be of invaluable assistance in providing a comprehensive view of the electronic interactions across the various oxidation/protonation states as well as the wealth of useful properties arising from the proton-coupled redox chemistry of these *apparently* simple triruthenium clusters.

Experimental Section

Chemical Preparations: The precursor complex $[Ru_3O(Ac)_6(py)_2(CH_3OH)]PF_6$ was prepared according to reported procedures.[5] All other reagents and solvents were of analytical grade and used as supplied. Britton–Robinson (BR) buffer solution (0.1 M) was employed in the pH-controlled experiments (pH 4–12). Sodium trifluoroacetate (NaTFA) or tetraethylammonium perchlorate (TEAP) was used as supporting electrolyte (I = 0.1 M) in sample solutions for (spectro)electrochemical measurements in water or acetonitrile, respectively.

$[Ru_3O(Ac)_6(py)_2(H_2O)]Cl$ was obtained by treating $[Ru_3O(Ac)_6(py)_2(CH_3OH)]PF_6$ (400 mg; 0.40 mmol) with $[AsPh_4]Cl$ (170 mg; 0.40 mmol) dissolved in water (30 mL), whilst stirring, for at least 2 h. The resulting white precipitate of $[AsPh_4]PF_6$ was collected on a fine filter containing microcrystalline cellulose, and the filtrate was roto-evaporated to dryness. The solid product was stored under vacuum. Yield: 230 mg (65%). $C_{22}H_{30}ClN_2O_{14}Ru_3$ (885.1): calcd. C 29.85, H 3.42, N 3.16; found C 28.77, H 3.35, N 3.29. IR (KBr, cm^{-1}): $\tilde{\nu}$ = 1556 m ($\upsilon_{as,}$ CO_2) , 1418 s (υ_s, CO_2) , 1607 m (υ_{ring}, py), 1485 m, and 1448 sh.

Physical Methods: Electronic spectra were recorded with either a HP 8453 diode-array spectrophotometer (UV/Vis) or a Guided Wave 260 fiber-optic instrument (near-IR). Cyclic voltammetry measurements were carried out with an Autolab PGSTAT 30 potentiostat/galvanostat and a conventional three-electrode cell containing a glassy-carbon working electrode (A = 0.196 cm^2), a platinum-wire auxiliary electrode, and an Ag/AgCl (1.0 M KCl, E^0 = 0.222 V vs. SHE) or $Ag/AgNO_3$ (0.010 M, E^0 = 0.503 V vs. SHE) reference minielectrodes in aqueous or acetonitrile solutions, respectively. A three-electrode system, arranged in a rectangular quartz cell (l = 0.25 mm), was used for the spectroelectrochemical measurements. In this case, a gold minigrid as a transparent working electrode was used with the above mentioned auxiliary and reference minielectrodes. All measurements were performed at room temperature (25 °C). Electrospray mass spectra were recorded with

a Micromass Q-Tof mass spectrometer with a quadrupole (Qq) and high-resolution orthogonal time of flight (o-TOF) configuration. Samples dissolved in pure methanol were injected using a syringe pump (Harvard Apparatus, Pump 11, 10 μL/min) through an uncoated fused-silica capillary. The ESI-MS mass spectra were acquired using an ESI capillary voltage of 3 kV and a cone voltage of 10 V.

Acknowledgments

The support from FAPESP, CNPq, RENAMI, IM2C, and CAPES/PICD is gratefully acknowledged.

[1] J. Burgess, *Metal Ions in Solution*, John Wiley & Sons, New York, **1978**.
[2] R. I. Cukier, D. G. Nocera, *Annu. Rev. Phys. Chem.* **1998**, *49*, 337–369.
[3] J. M. Mayer, *Annu. Rev. Phys. Chem.* **2004**, *55*, 363–390.
[4] T. J. Meyer, M. H. V. Huynh, *Inorg. Chem.* **2003**, *42*, 8140–8160.
[5] H. E. Toma, K. Araki, A. D. P. Alexiou, S. Nikolaou, S. Dovidauskas, *Coord. Chem. Rev.* **2001**, *219–221*, 187–234.
[6] A. Spencer, G. Wilkinson, *J. Chem. Soc., Dalton Trans.* **1972**, 1570–1577.
[7] A. Spencer, G. Wilkinson, *J. Chem. Soc., Dalton Trans.* **1974**, 786–792.
[8] S. T. Wilson, R. F. Bondurant, T. J. Meyer, D. J. Salmon, *J. Am. Chem. Soc.* **1975**, *97*, 2285–2287.
[9] J. A. Baumann, D. J. Salmon, S. T. Wilson, T. J. Meyer, W. E. Hatfield, *Inorg. Chem.* **1978**, *17*, 3342–3350.
[10] H. E. Toma, C. Cipriano, *J. Electroanal. Chem.* **1989**, *263*, 313–322.
[11] H. E. Toma, C. J. Cunha, *Can. J. Chem.* **1989**, *67*, 1632–1635.
[12] B. A. Moyer, T. J. Meyer, *Inorg. Chem.* **1981**, *20*, 436–444.
[13] V. R. Souza, G. S. Nunes, R. C. Rocha, H. E. Toma, *Inorg. Chim. Acta* **2003**, *348*, 50–56.
[14] E. L. Lebeau, S. A. Adeyemi, T. J. Meyer, *Inorg. Chem.* **1998**, *37*, 6476–6484.
[15] R. C. Rocha, H. E. Toma, *Quim. Nova* **2002**, *25*, 624–638.
[16] B. A. Moyer, M. S. Thompson, T. J. Meyer, *J. Am. Chem. Soc.* **1980**, *102*, 2310–2312.
[17] M. S. Thompson, W. F. Degiovani, B. A. Moyer, T. J. Meyer, *J. Org. Chem.* **1984**, *49*, 4972–4977.
[18] J. C. Dobson, W. K. Seok, T. J. Meyer, *Inorg. Chem.* **1986**, *25*, 1513–1514.
[19] K. Y. Wong, C. M. Che, F. C. Anson, *Inorg. Chem.* **1987**, *26*, 737–741.
[20] L. Roecker, T. J. Meyer, *J. Am. Chem. Soc.* **1987**, *109*, 746–754.
[21] C. M. Che, V. W. W. Yam, *J. Am. Chem. Soc.* **1987**, *109*, 1262–1263.
[22] M. E. Marmion, K. J. Takeuchi, *J. Am. Chem. Soc.* **1988**, *110*, 1472–1480.
[23] C. M. Che, W. T. Tang, W. T. Wong, T. F. Lai, *J. Am. Chem. Soc.* **1989**, *111*, 9048–9056.
[24] C. M. Che, V. W. W. Yam, T. C. W. Mak, *J. Am. Chem. Soc.* **1990**, *112*, 2284–2291.
[25] C. M. Che, C. Ho, T. C. Lau, *J. Chem. Soc., Dalton Trans.* **1991**, 1901–1907.
[26] C. M. Che, W. T. Tang, W. O. Lee, K. Y. Wong, T. C. Lau, *J. Chem. Soc., Dalton Trans.* **1992**, 1551–1556.
[27] Y. K. Lai, K. Y. Wong, *Electrochim. Acta* **1993**, *38*, 1015–1021.
[28] A. S. Kanmani, S. Vancheesan, *J. Mol. Catal. A* **1997**, *125*, 127–134.
[29] M. Navarro, W. F. Degiovani, J. R. Romero, *J. Mol. Catal. A* **1998**, *135*, 249–256.
[30] E. L. Lebeau, T. J. Meyer, *Inorg. Chem.* **1999**, *38*, 2174–2181.
[31] D. Chatterjee, A. Mitra, R. E. Shepherd, *Inorg. Chim. Acta* **2004**, *357*, 980–990.
[32] R. S. Nicholson, I. Shain, *Anal. Chem.* **1964**, *36*, 706–722.
[33] D. T. Sawyer, A. Sobkowiak, J. L. Roberts Jr, *Electrochemistry for Chemists*, John Wiley & Sons, New York, **1995**.
[34] A. Gerli, J. Reedijk, M. T. Lakin, A. L. Spek, *Inorg. Chem.* **1995**, *34*, 1836–1843.
[35] K. J. Takeuchi, M. S. Thompson, D. W. Pipes, T. J. Meyer, *Inorg. Chem.* **1984**, *23*, 1845–1851.

Received: December 6, 2005
Published Online: February 15, 2006

